Numerical and experimental study of the vibrational modes of thermally prestressed and prebent beams

Fabien Treyssede

ICSV13 - Vienna
The Thirteenth International Congress on Sound and Vibration
Vienna, Austria, July 2-6, 2006

NUMERICAL AND EXPERIMENTAL STUDY OF THE VIBRATIONAL MODES OF THERMALLY PRESTRESSED AND PREBENT BEAMS

Fabien Treyssède*[1]

[1]Laboratoire Central des Ponts et Chaussées, Service Métrologie et Instrumentation, Route de Pornic, BP 4129, 44341 Bouguenais Cedex, France
fabien.treyssede@lcpc.fr

Abstract

In this paper, the linear vibrations of thermally prestressed beams are studied, including the prebending effects. General equations governing structural vibrations superimposed on an initial static state are first given. They are applied to a planar Euler-Bernoulli beam under the assumption of small prestrain and large predisplacement. Initial imperfections are included in the whole analysis. The governing equilibrium equations are solved using a finite element method. This model is then validated through experiments inside a climatic chamber.

INTRODUCTION

For thin structures such as beams or plates, the effects of prestress are likely to have a significant impact upon the structural dynamical behaviour. On the contrary of fully thick structures, this occurs even for relatively low prestress states, far from the buckling stage, because of an amplifying factor given by the slender ratio. As far as beams are concerned, it is well known that the natural frequencies of flexural vibration increase (resp. decrease) when the axial load is tensile (resp. compressive) [1].

Nevertheless, most of studies found in the litterature deal exclusively with in-plane prestress effects, whereas prestressed states generally induce some prebending, yielding a predeformed geometry. To the author knowledge, the prebending effects are hardly studied and often neglected, particularly for low prestress states, so that their effects upon vibrations remain obscure. In this paper, the linear vibrations of prestressed planar beams including prebending effects are studied. Without loss of generality, this paper focus on thermal prestressing, in the context of structural health monitoring based on modal diagnosis with thermal compensation [2] and the need of

adequate numerical models. A typical application of civil structures is a bridge subjected to climatic thermal variations [3].

GENERAL EQUATIONS

In prestressed dynamics, three configurations must be distinguished: the reference configuration (undeformed and unprestressed), the predeformed configuration (corresponding to the prestress state), and the total configuration (including superimposed dynamical deformations). Quantities referring to these configurations will respectively be denoted with a subscript *ref*, a subscript 0 and a tild. The absence of symbol will be left for superimposed dynamical quantities. In this paper, the reference configuration represents the ideal geometry, without initial imperfections, denoted by the subscript *i*.

We restrict our study to conservative systems, linear thermoelastic constitutive laws, static (or quasi-static) prestress states, and small superimposed vibrations. The prestress/predeformation effects are viewed by dynamics through the geometric nonlinearities of the prestress state. Mechanically induced heating is neglected, as well as thermally induced vibrations.

Based on a Lagrangian formulation [4], Hamilton's principle for the total configuration is written in terms of the following total kinetic energy, total strain energy and external energy:

$$\tilde{T}=\frac{1}{2}\int_{\Omega_{ref}}\rho_{ref}\dot{\tilde{\mathbf{u}}}\cdot\dot{\tilde{\mathbf{u}}}d\Omega \;\;;\;\; \tilde{V}=\frac{1}{2}\int_{\Omega_{ref}}\tilde{\mathbf{E}}:\tilde{\mathbf{S}}d\Omega \;\;;\;\; \tilde{V}_{ext}=-\int_{\Omega_{ref}}\rho_{ref}\tilde{\mathbf{u}}\cdot\tilde{\mathbf{f}}d\Omega-\int_{\Gamma_{ref}^{T}}\tilde{\mathbf{u}}\cdot\bar{\bar{\mathbf{T}}}d\Gamma \qquad (1)$$

Within the scope of linear thermoelasticity, the stress and strain tensors are related through $\tilde{\mathbf{S}}=\boldsymbol{\Lambda}:\tilde{\mathbf{E}}-\boldsymbol{\kappa}\theta_0$. In the presence of initial imperfections $\mathbf{u_i}$ (which are supposed to be known), the Green-Lagrange strain tensor must also include some imperfection terms, and is written as $\tilde{\mathbf{E}}=1/2\left(\nabla\tilde{\mathbf{u}}+\nabla\tilde{\mathbf{u}}^T+\nabla\tilde{\mathbf{u}}^T\nabla\tilde{\mathbf{u}}+\nabla\mathbf{u_i}^T\nabla\tilde{\mathbf{u}}+\nabla\tilde{\mathbf{u}}^T\nabla\mathbf{u_i}\right)$.

Now, the total displacement vector is decomposed as a sum of two components, one corresponding to the prestress state, and the other corresponding to small superimposed non-stationary perturbations. Applying this decomposition into (1), and keeping only quadratic terms in $\mathbf{u}$ (for the purpose of linearisation), Hamilton's principle holds for the superimposed dynamic state, with the following energy expressions:

$$T=\frac{1}{2}\int_{\Omega_{ref}}\rho_{ref}\dot{\mathbf{u}}\cdot\dot{\mathbf{u}}d\Omega \;\;;\;\; V=\frac{1}{2}\int_{\Omega_{ref}}\mathbf{E}:\mathbf{S}d\Omega+\frac{1}{2}\int_{\Omega_{ref}}\mathrm{tr}\left(\nabla\mathbf{u}\cdot\mathbf{S_0}\cdot\nabla\mathbf{u}^T\right)d\Omega \;\;;\;\; V_{ext}=-\int_{\Omega_{ref}}\rho_{ref}\mathbf{u}\cdot\mathbf{f}d\Omega-\int_{\Gamma_{ref}^{T}}\mathbf{u}\cdot\bar{\mathbf{T}}d\Gamma \qquad (2)$$

$\mathbf{S}$ is the second Piola-Kirchoff stress increment tensor ($\mathbf{S}=\boldsymbol{\Lambda}:\mathbf{E}$). $\mathbf{E}$ is the linearised Green-Lagrange strain increment tensor: $\mathbf{E}=1/2\left(\nabla\mathbf{u}+\nabla\mathbf{u}^T+\left(\nabla\mathbf{u_0}+\nabla\mathbf{u_1}\right)^T\nabla\mathbf{u}+\nabla\mathbf{u}^T\left(\nabla\mathbf{u_0}+\nabla\mathbf{u_1}\right)\right)$.

In non-linear mechanics, the formulation (2) is referred to as the total Lagrangian formulation, here in its linearised version [5]. In the present study, one advantage of such a formulation is that the predeformation effects appear explicitly through $\mathbf{u_0}$, for more physical insights.

APPLICATION TO PLANAR BEAMS

The equations governing the dynamic equilibrium of a planar Euler-Bernoulli beam are derived from a total Lagrangian formulation. Small prestrain and large predisplacement are assumed. The beam axis, denoted *x*, is not necessarily a neutral axis. The axis corresponding to the direction of transverse diplacements is denoted *z*. In the remaining of this paper, *x* derivatives will be denoted by $(.)_{,x}$. An isotropic material is supposed. Then, the following expressions hold:

$$\tilde{E}_{xx} = \left(\tilde{u} - z\tilde{w}_{,x}\right)_{,x} + \frac{1}{2}\tilde{w}_{,x}{}^2 + w_{i,x}\tilde{w}_{,x} \quad ; \quad \tilde{S}_{xx} = E\left(\tilde{E}_{xx} - \alpha\theta_0\right) \tag{3}$$

E and α are respectively the Young's modulus and the coefficient of thermal expansion. Now, it can be shown that the application of Hamilton's principle (1) yields the equilibrium equations, together with the expressions of the axial force, the moment and the transverse force resultants:

$$\begin{cases} \tilde{N}_{,x} + \tilde{\tilde{t}}_x = \rho_m \ddot{\tilde{u}} - \rho_{mf} \ddot{\tilde{w}}_{,x} \\ \tilde{Q}_{,x} + \left(\left(\tilde{w}_{,x} + w_{i,x}\right)\tilde{N}\right)_{,x} + \tilde{\tilde{t}}_z = \rho_m \ddot{\tilde{w}} \end{cases} \text{ with: } \begin{cases} \tilde{N} = \int_A \tilde{S}_{xx} dA = H_m\left(\tilde{u}_{,x} + \frac{1}{2}\tilde{w}_{,x}{}^2 + \tilde{w}_{,x} w_{i,x}\right) - H_{mf}\tilde{w}_{,xx} - \int_A E\alpha\theta_0 dA \\ \tilde{M} = \int_A z\tilde{S}_{xx} dA = H_{mf}\left(\tilde{u}_{,x} + \frac{1}{2}\tilde{w}_{,x}{}^2 + \tilde{w}_{,x} w_{i,x}\right) - H_f\tilde{w}_{,xx} - \int_A E\alpha\theta_0 z dA \\ \tilde{Q} = \tilde{M}_{,x} + \tilde{\tilde{m}} - \rho_{mf}\ddot{\tilde{u}} + \rho_f \ddot{\tilde{w}}_{,x} \end{cases} \tag{4}$$

A denotes the cross-sectional area in the reference configuration, and ∂A is its contour. The prestress state verifies Eqs. (4) for the static case. The following notations have been used:

$$\begin{gathered} \left(H_m, H_{mf}, H_f\right) = \int_A E\left(1, z, z^2\right) dA \quad ; \quad \left(\rho_m, \rho_{mf}, \rho_f\right) = \int_A \rho_{ref}\left(1, z, z^2\right) dA \\ \tilde{\tilde{t}}_x = \int_A \rho_{ref}\tilde{f}_x dA + \int_{\partial A}\tilde{\tilde{T}}_x ds \quad ; \quad \tilde{\tilde{t}}_z = \int_A \rho_{ref}\tilde{f}_z dA + \int_{\partial A}\tilde{\tilde{T}}_z ds \quad ; \quad \tilde{\tilde{m}} = \int_A \rho_{ref}\tilde{f}_x z dA + \int_{\partial A}\tilde{\tilde{T}}_x z ds \end{gathered} \tag{5}$$

From (2) and by neglecting the terms of higher order effects, it can be shown that the following energies can be obtained for the superimposed dynamic state:

$$\begin{cases} T = \frac{1}{2}\int_0^L \rho_m\left(\dot{u}^2+\dot{w}^2\right)dx + \frac{1}{2}\int_0^L \rho_f \dot{w}_{,x}{}^2 dx - \int_0^L \dot{u}\rho_{mf}\dot{w}_{,x}dx \\ V_{ext} = -\int_0^L u\bar{t}_x dx - \int_0^L w\bar{t}_z dx + \int_0^L w_{,x}\bar{m}dx - \left[u\int_A \bar{T}_x dA + w\int_A \bar{T}_z dA - w_{,x}\int_A z\bar{T}_x dA\right]_0^L \\ V = \frac{1}{2}\int_0^L H_m u_{,x}{}^2 dx + \frac{1}{2}\int_0^L H_f w_{,xx}{}^2 dx - \int_0^L u_{,x}H_{mf}w_{,xx}dx + \frac{1}{2}\int_0^L N_0 w_{,x}{}^2 dx \\ \quad + \int_0^L u_{,x}H_m\left(w_{0,x}+w_{i,x}\right)w_{,x}dx - \int_0^L w_{,x}H_{mf}\left(w_{0,x}+w_{i,x}\right)w_{,xx}dx + \frac{1}{2}\int_0^L H_m\left(w_{0,x}+w_{i,x}\right)^2 w_{,x}{}^2 dx \end{cases} \quad (6)$$

The application of Hamilton's principle gives the equilibrium equations for prestress dynamics (not shown here for conciseness). It can be verified that they exactly correspond to a direct linearisation of Eqs. (4). The incremental strain energy V is dependent of two prestress variables: the "classical" axial preload N_0, and the predisplacement derivative $w_{0,x}+w_{i,x}$. Hence for dynamics, the predisplacement due to prebending must be summed with that due to initial imperfections.

NUMERICAL METHOD

The above equations are solved using a FE method. In a conventional manner, a linear interpolation is chosen for the axial displacement and the geometry. Hermitian interpolation functions are used for approximating the transversal displacement. The elements have three degrees of freedom per node associated to u, w, $-w_{,x}$.

Prestress State

The prestress state is obtained by solving the static non-linear system (4), denoted $\mathbf{K_0(U_0)U_0=F_0}$ after FE discretisation. This system may be efficiently solved with an iterative algorithm of Newton-Raphson type [6], by computing successive incremental displacement given by: $\mathbf{K_T}^{j-1}\delta\mathbf{U} = \mathbf{R}^{j-1}$, where $\mathbf{K_T}$ is the tangential stiffness matrix and $\mathbf{R}$ is the residue. The superscript j-1 denotes the step number in the iterative process. The next step j is given by: $\mathbf{U_0}^j = \mathbf{U_0}^{j-1} + \delta\mathbf{U}$.

Dynamics

After discretising expressions (6) and assembling, the application of Hamilton's principle yields the algebraic system: $\mathbf{M\ddot{U}} + \mathbf{KU} = \mathbf{F}$, where $\mathbf{K}$ and $\mathbf{M}$ are symmetric matrices. In this paper, we will focus on eigenmodes, given by $\left(\mathbf{K} - \omega^2\mathbf{M}\right)\mathbf{U} = \mathbf{0}$.

$\mathbf{K}$ is dependent on N_0 and w_0+w_i and may be decomposed as a sum of three matrices $\mathbf{K_{lin}}+\mathbf{K_\sigma}+\mathbf{K_L}$ defined, from V in Eqs. (6), as follows. $\mathbf{K_{lin}}$ represents the small displacement stiffness matrix, usual in linear analysis. $\mathbf{K_\sigma}$ is a matrix, often

called the geometric stiffness matrix, dependent on the axial prestress level. $\mathbf{K_L}$ is a matrix due to the presence of predisplacement. The whole matrix **K** may be not definite positive when buckling occurs (but as stated earlier, we are interested in low prestress states far from the buckling stage). **K** may also be directly obtained from the prestress state computation because it exactly corresponds to the tangential stiffness matrix.

EXPERIMENTAL SETUP

The experimental device is depicted in Fig. 1. A vertical test beam is clamped at both ends on a workbench made of four vertical thick columns and two horizontal decks. This workbench is made of steel, whereas the beam is made of aluminium. The whole apparatus is set inside a climatic chamber with controlled ambient temperature.

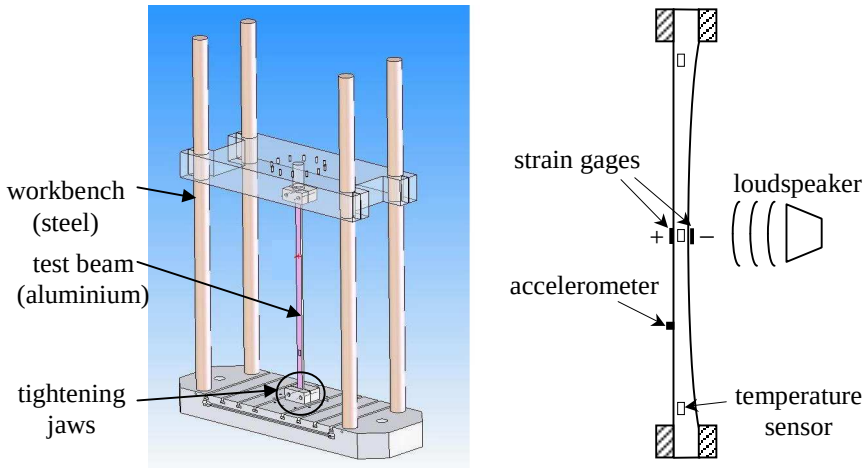

Figure 1 – Workbench (left) and instrumented test beam (right)

Because steel and aluminium do not have the same coefficient of thermal expansion (1.17e–5 and 2.30e–5 K^{-1} respectively), a temperature change will naturally induce a significant axial prestress inside the beam. From Eqs. (4), this quasi-static prestress N_0 is constant along the beam, even though a temperature gradient might exist along the beam.

One considers a beam of length L=1 m and 0.03 m depth. As sketched in Fig.1, the beam profile is circular, so that no straight neutral axis exists. The thickness varies from 0.03 m at extremities to 0.01 m at center. The cross-section is rectangular. The material properties are E=7.24e+10 Pa, ρ=2790 kg/m^3. Those characteristics have been experimentally checked by comparing theoretical and experimental, free-free and clamped-free eigenfrequencies. For a better match with the experimental boundary conditions, a torsional spring is used in the model at both ends (with stiffness C=3e5 N.m).

As depicted in Fig. 1, the beam has been instrumented with one accelerometer, a pair of aluminium strain gages with thermal compensation and some temperature

sensors. Under the assumption of small strain, the gages provide a measurement of the compensate strains at the upper (+) and lower (-) sides. With the uniformity of the temperature on the beam cross-section (the Biot number is less than 0.1), the curvature $w_{0,xx}(L/2)$ and the axial prestress N_0 are respectively obtained from the difference divided by thickness and the half sum of strains divided by H_m. N_0 can thus be experimentally obtained without requiring any temperature sensor (and only at one measurement point because it remains axially constant).

Tests are carried out inside the climatic chamber, first by stabilizing the ambient temperature for 3 hours, and then heating for 27 hours with a slope of +1°C per hour. The beam is acoustically excited by a loudspeaker with a white noise input. Strain and temperature measurements are saved every seconds. Acceleration measurements are automatically triggered every thirty minutes, for 250 seconds with a 1280Hz sampling frequency. Some experimental results are given in Fig.2. They clearly show that the first eigenfrequency decreases as the average temperature increases versus time, whereas the axial prestress and the curvature decrease.

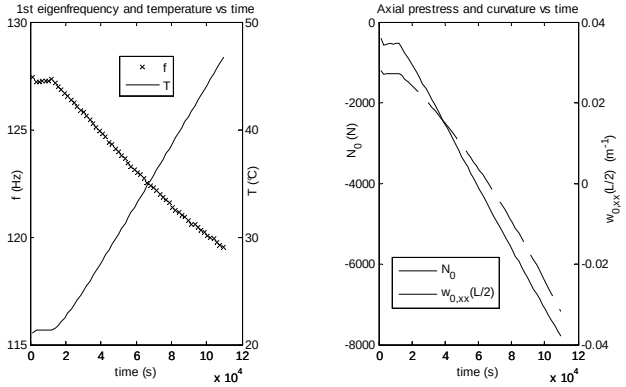

Figure 2 – Experimental results vs. time : averaged beam temperature and 1st eigenfrequency (left), axial prestress and center curvature (right).

RESULTS

Prestress State

The knowledge of N_0 and $w_0(x)+w_i(x)$ is a crucial step. First, the initial imperfections have been measured with an optical displacement sensor and then interpolated on each node. Between both ends, a non negligible difference of 5.5 mm was observed. The computation of the prestress state would *a priori* require the knowledge of the complete temperature field inside the beam. However, in the test-case considered, there is no prebending load (because the temperature is cross-sectionally constant in particular), which means that the knowledge of N_0 is sufficient to determine the whole predeformed state.

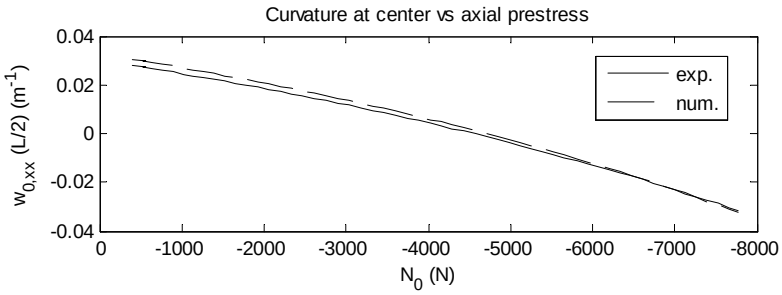

Figure 3 – experimental (solid line) and computed (dashed line) curvatures at center.

In the FE model, the boundary conditions are as follows. A zero axial predisplacement is enforced at one extremity while the measured axial prestress is enforced at the other. At the end, w_0 is enforced to zero because the jaws position has been carefully adjusted to the imperfect beam in the experiment. Besides, some constant angles are taken into account at both ends of the beam, because tightening jaws are not perfectly perpendicular (both angles were found from the measurement of the predeformed beam in its clamped-clamped configuration). Fig. 3 provides a satisfying comparison of the evolutions of experimental and FE curvatures at center throughout the test.

Eigenfrequencies

In this example, we will exclusively focus on eigenfrequencies because the sensitivity of modal shapes with prestress in the FE model was found to be quite negligible.

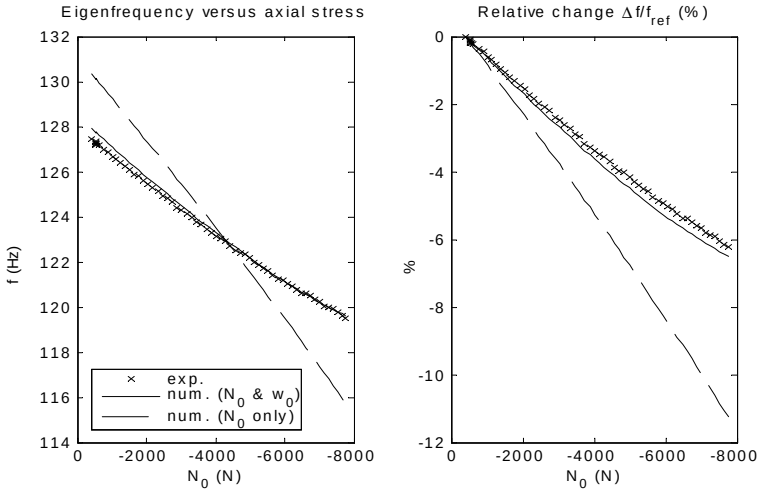

Figure 4 – Left: 1st eigenfrequency vs. axial prestress: experimental (x), computed with prebending (solid line) and without (dashed line). Right : relative change vs. axial prestress.

Figure 4 depicts the change in the first eigenfrequency with the axial prestress during the test. In the experiment, a decrease from 127.5 Hz to 119.5 Hz is observed. The comparison between experimental and numerical results clearly demonstrates the influence of prebending: if only the axial prestress is considered in the computation of

this eigenfrequency, a significant difference with the experiment is found. The relative change in frequency with respect to the reference (corresponding to the beginning of the test) decreases to −6% at the end of the experiment, as well as in the FE model based on a complete prestress state. Without prebending, the numerical results give an erroneous change of about −11%. The evolutions of eigenfrequencies of modes 2 and 3 have also been analysed (not shown here for conciseness). The mode 2 (resp. 3) varies from 264.7 Hz (resp. 467.8 Hz) to 245.0 Hz (resp. 445.3 Hz), yielding a relative change of −7.3% (−4.8%) at the end of the experiment. This relative change is in good agreement with the FE model, with or without prebending, indicating that these modes are not sensitive to prebending.

CONCLUSIONS

From the results above, when the predeformation is neglected, the axial prestress has a stronger shifting effect for lower eigenfrequencies. This is coherent with the standard results found in the litterature [1]. Nevertheless, this statement might not be true anymore in the presence of significant prebending, which tends to reduce the shifting effects of axial prestress upon some isolated modes (the first one, in the example presented). In practice, neglecting prebending in eigenfrequency computations may lead to errors of several percents, even when the predisplacement remains relatively small compared to the beam length (less than 0.5% in the experiment).

Acknowledgement

This research was partially supported by the project CONSTRUCTIF, in the framework of the French Computer and Security program (ACI S&I).

REFERENCES

[1] Bokaian, “Natural frequencies of beams under compressive axial loads”, Journal of Sound and Vibration **126** (1988) 49-65.

[2] H. Sohn, M. Dzwonczyk, E.G. Straser, A.S. Kiremidjian, K.H. Law, T. Meng, “An experimental study of temperature effects on modal parameters of the Alamosa canyon bridge”, Earthquake Engineering and Structural Dynamics **28** (1999) 879-897.

[3] R.G. Rohrmann, M. Baessler, S. Said, W. Schmid, W.F. Ruecker, “Structural causes of temperature affected modal data of civil structures obtained by long time monitoring”, Proceedings of the International Modal Analysis Conference (IMAC), San Antonio, USA, 2000, pp. 1-7.

[4] K. J. Bathe, *Finite Element Procedures* (Prentice Hall, Englewood Cliffs, 1996).

[5] Y.-B. Yang, S.-R. Kuo, *Nonlinear Framed Structures* (Prentice Hall, Singapore, 1994).

[6] O. C. Zienkiewicz, R. L. Taylor, *The Finite Element Method – Vol. 2 : Solid and Fluid Mechanics, Dynamics and Non-Linearity* (McGraw-Hill, London, 1998).